Electronic damage in quartz (c-SiO_2) by MeV ion irradiations: Potentiality for optical waveguiding applications

J. Manzano-Santamaría , J. Olivares , A. Rivera , F. Agulló-López

A B S T R A C T

The damage induced on quartz (c-SiO_2) by heavy ions (F, O, Br) at MeV energies, where electronic stopping is dominant, has been investigated by RBS/C and optical methods. The two techniques indicate the formation of amorphous layers with an isotropic refractive index (n = 1.475) at fluences around 10^{14} cm ^{2} that are associated to electronic mechanisms. The kinetics of the process can be described as the superposition of linear (possibly initial Poisson curve) and sigmoidal (Avrami-type) contributions. The coexistence of the two kinetic regimes may be associated to the differential roles of the amorphous track cores and preamorphous halos. By using ions and energies whose maximum stopping power lies inside the crystal (O at 13 MeV, F at 15 MeV and F at 30 MeV) buried amorphous layer are formed and optical waveguides at the sample surface have been generated.

1. Introduction

Quartz (c-SiO_2) is an interesting crystalline non-centrosymmetric material with trigonal symmetry (point group 32). For photonic applications, it has a broad transparency range with fundamental optical edge at around 200 nm. Although the nonlinear optical coefficients are small, it may be applied for second harmonic generation devices [1]. Many studies of radiation damage with a variety of sources (X-rays, electrons, light ions) have been performed and the comparison to (amorphous) silica (a-SiO_2) offers an interesting route to investigate the role of crystallinity on defect generation. For both materials, a number of point defects and colour centres (E', NBOH, etc.) can be generated and are reasonably well understood [2–4]. More recently, the effect of irradiation with energetic (MeV) heavy ions having a dominant electronic stopping power is being investigated. It has been shown that the induced damage has peculiar features in comparison to that caused by nuclear elastic collisions. In particular, nanometer-diameter tracks of higher density (compact) material have been observed in silica [5,6] for ion irradiations with stopping powers above a certain threshold (1–2 keV/nm). For quartz, tracks containing amorphized material are formed [7] above similar thresholds. In fact, the compaction effect and the corresponding refractive index increase caused on silica by those ions have allowed for the fabrication of non-tunnelling optical waveguides at the sample surface [8]. For quartz substrates, optical waveguides have been produced by light ion implantation [9], i.e. in the nuclear stopping regime, but the application of heavy energetic ions for photonic purposes has not been so far reported.

The purpose of this work has been to obtain systematic kinetic data on the damage induced on quartz by heavy swift ions having a broad span of electronic stopping powers. However, in contrast to previous works, where irradiations showed a strong competition of electronic and nuclear processes [10], we are in the dominant electronic regime. An interesting kinetic behaviour has been revealed suggesting the combination of Poisson and (sigmoidal) Avrami-type kinetics [11,12], whose relative contributions depend on electronic stopping power. As for photonic applications, the irradiation induces a decrease in density and so it is not, in principle, adequate for the production of optical waveguides as achieved in the case of silica. However, we have used here a novel strategy that was successfully applied in the case of $LiNbO_3$ [13] and $KGd(WO_4)_2$ or KGW [14]. The idea is to irradiate with ions whose stopping power reaches a maximum inside the crystal and defines a crystalline quality waveguide at the surface. Results are quite promising for future photonic devices.

2. Experimental

Synthetic quartz plates, purchased from Crystran, were irradiated with different ions and energies that are listed in Table 1 to-

Table 1
Ions and energies used during irradiations. The corresponding electronic stopping powers, S_e, at the surface of the sample are also listed.

Ion	Energy (MeV)	S_e (keV/nm)
Fluorine	5	2.5
Fluorine	15	2.3
Oxygen	4	2.1
Oxygen	13	1.9
Bromine	25	6.8
Bromine	40	8

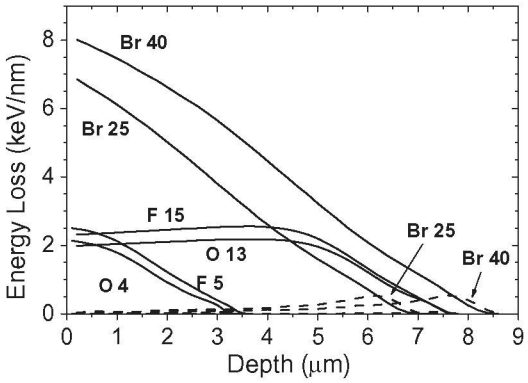

Fig. 1. Electronic stopping power (continuous line) for fluorine, oxygen and bromine for different energies (indicated in the figure) as a function of depth in quartz. For Br (25 MeV) and Br (40 MeV), the nuclear stopping power is shown (dashed line) for comparison.

gether with the electronic and nuclear stopping power at the sample surface. The irradiations were performed at the 5 MV tandetron accelerator installed at CMAM. The stopping powers as a function of depth are illustrated in Fig. 1 showing that the stopping powers in the first few microns of depth from the surface is essentially electronic. One should note that for F 15 MeV and O 13 MeV the maximum of the electronic stopping power, where the heavy disorder (amorphization) is thought to be initiated, lies inside the sample. They will be used for waveguide fabrication. The other irradiations at F 5 MeV, O 4 MeV and Br 25 and 40 MeV will be used to investigate the mechanisms and kinetics of damage. The disorder induced in the crystal lattice was measured by RBS/C channelling experiments using He at around 3 MeV. Details of the technique that compares the RBS yield under random or channelled incidence can be consulted in some references [11,15]. Optical waveguiding was investigated by the dark-mode method (at a wavelength of 633 nm) using a high index glass prism [13]. The refractive index profiles induced by irradiation were obtained from the observed propagating modes by a Wentzel–Kramers–Brillouin (WKB) method [16].

3. Evolution of damage with irradiation fluence

The evolution of the irradiation-induced disorder at the sample surface has been investigated by following the standard procedures from the raw RBS/C spectra such as illustrated in Fig. 2. Results for the normalized disordered area as a function of fluence are plotted in Fig. 3a (for F 5 MeV, F 15 MeV, O 4 MeV and O 13 MeV) and Fig. 3b (for Br 25 MeV and Br 40 MeV). One sees that the fluence scales are very different, indicating that the damage efficiency is much higher for the second case where the electronic stopping power is higher. The damage growth curves in Fig. 3a present a very interesting behaviour. They consist of an initial stage of linear growth followed by a strongly rising slope after a given incubation fluence. This behaviour cannot be related to the damage expected

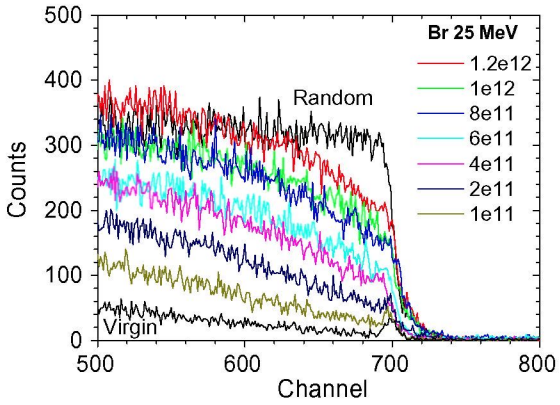

Fig. 2. Representative RBS/C spectra measured with a probe ion beam of He 3 MeV, corresponding to the irradiations with bromine 25 MeV for the (seven) fluences indicated in the figure in units of cm^{-2}. From the lowest (1×10^{11} cm^{-2}) to the highest (1.2×10^{12} cm^{-2}) fluence, the damage level increases with the fluence.

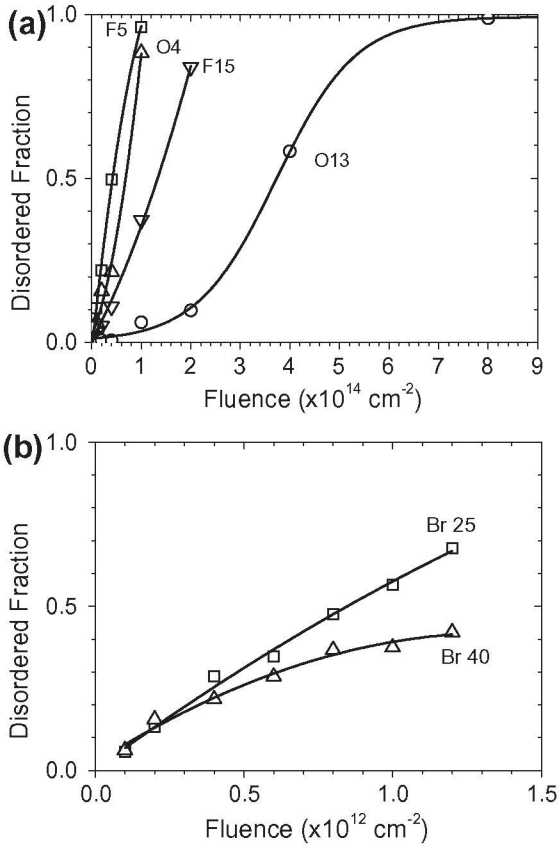

Fig. 3. Evolution of the normalized disordered area at the sample surface as a function of fluence for (a) F (5 MeV and 15 MeV) and O (4 MeV and 13 MeV) and (b) Br (25 MeV and 40 MeV).

from the elastic nuclear collisions and has to be mostly ascribed to electronic processes. The initial stage may correspond to the linear part of a Poisson kinetics expected from the overlapping of the amorphous tracks generated by the ion impacts [17]. The curves in Fig. 3b only show the monotonic rise typical of Poisson behaviour although a detailed analysis has not been performed. From the curves in Fig. 3 we have derived the initial slope of the amorphization kinetics (i.e. *the damage cross-section*) that is plotted as a function of the electronic stopping power in Fig. 4. The curve is strongly superlinear as predicted by electronic mechanisms [17,18] and can be extrapolated to show the existence of an elec-

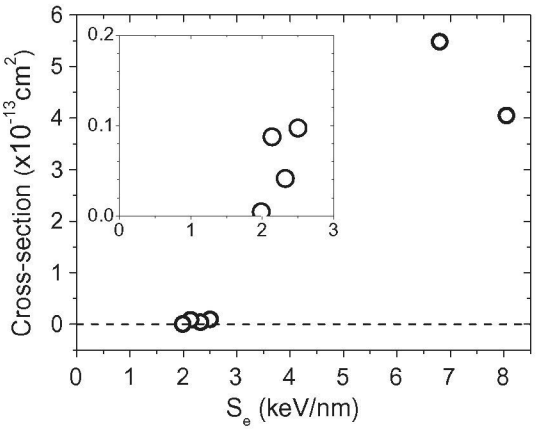

Fig. 4. Evolution of the initial disordering rate (damage cross-section) as function of the electronic stopping power. N_o and N_e stand, respectively, for the ordinary and extraordinary refractive indices. The inset provides a zoom for the stopping power region close to threshold.

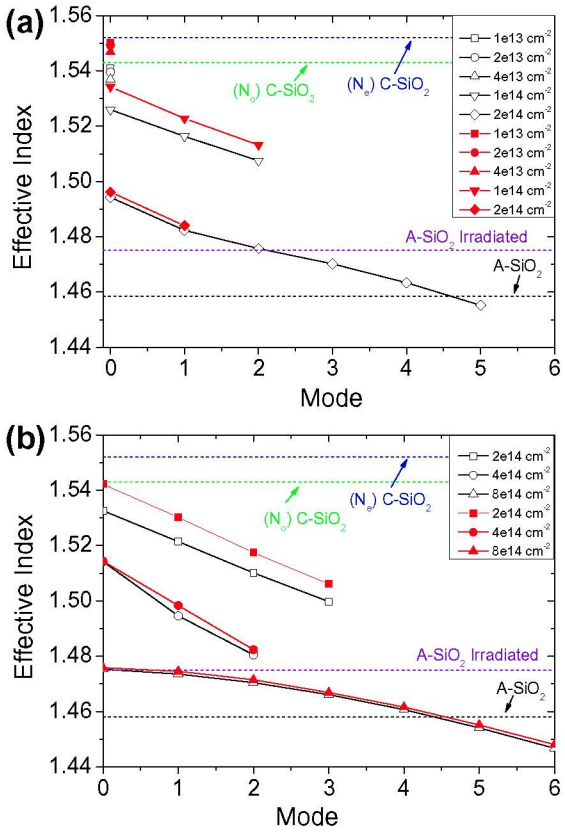

Fig. 5. Effective indices (at 633 nm wavelength) obtained using the darkmode method, for F 15 MeV (a) and O 13 MeV (b) open and close symbols correspond with TE and TM polarization, respectively. The ordinary and extraordinary refractive indices, N_o and N_e respectively, of the c-SiO_2 substrate are indicated with dashed lines. The refractive indices of the virgin amorphous silica (a-SiO_2) and of the irradiated a-SiO_2 are also shown with dashed lines.

tronic stopping threshold around or below 2 keV/nm which is close to values previously reported [7].

4. Optical waveguides

For the production of optical waveguides, we have followed the strategy proposed and satisfactorily tested for $LiNbO_3$ and KGW

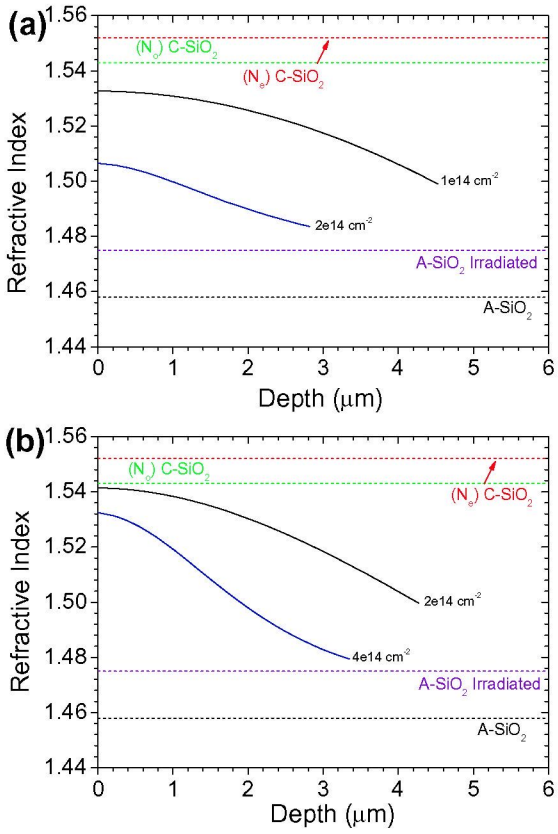

Fig. 6. Refractive index profiles obtained for the irradiations with F 15 MeV (a) and O 13 MeV (b), for the fluences indicated in the labels (in units of ions/cm^2).

that uses ions whose maximum electronic stopping power lies inside the crystal [13,14]. The TE and TM modes measured in F 15 MeV and O 13 MeV are, respectively, shown in Fig. 5, indicating a clear anisotropy. The refractive index profiles derived from those modes are displayed in Fig. 6. It is clear that a small reduction in refractive index occurs at the surface but the index decreases rapidly when approaching the maximum of electronic stopping power for a depth of around 4–5 μm. The final refractive index value at this depth very closely approaches the isotropic value, $n = 1.475$, corresponding to saturation of swift-ion irradiated a-SiO_2 [8] and suggests that the crystal becomes amorphized. One should note that at such depth the nuclear damage can be neglected and therefore the effect is of a purely electronic origin. It is interesting to observe that the final refractive index caused either by irradiating crystalline (quartz) or amorphous silica is the same (around 1.475) and should correspond to the equilibrium amorphous state of SiO_2 under irradiation.

5. Discussion

All damage growth curves present an initial finite slope even for the lowest stopping powers, suggesting that in all cases we are above the threshold, that should be, then, slightly below 2 keV/nm. Except at the highest stopping power (Br at 25 MeV and 45 MeV), the shape of the damage curves is not Poisson but it can be qualitatively analysed in terms of a Poisson plus a sigmoidal kinetics. The Poisson component accounts for the initial linear growth whereas the sigmoidal kinetics could be related to an Avrami kinetics (with a zero initial slope) that has been, indeed, observed in many irradiation cases [11,12] below or slightly above threshold. Although a more quantitative analysis should be performed, we attribute the observed behaviour to the complex struc-

ture of tracks, consisting of an amorphous core and a defective (preamorphous) halo. This structure has been inferred from a number of experiments and it has been simulated for $LiNbO_3$ with an accumulative MonteCarlo model [17] based on the non-radiative decay of localized excitons [19,20]. The initial slope of the Poisson kinetics at low fluences can be interpreted in terms of isolated amorphous track cores and permits the determination of the amorphization cross-section (Fig. 3). On the other hand, the later Avrami stage, only observed in Fig. 3a, presents a clear incubation fluence and may be caused by the overlapping of the preamorphous halos (yielding a zero initial slope) as justified by the MonteCarlo approach in Ref. [17]. The microscopic damage mechanism for quartz is not yet clear although it could be excitonic. However, the self-trapping of excitons in quartz has not been yet assessed, although defects in amorphous silica can be generated by non-radiative decay of self-trapped excitons [21].

6. Summary and conclusions

The damage and amorphization kinetics of quartz under ion-beam irradiation in the electronic stopping regime has been determined by RBS/C. A threshold for amorphization can be identified at around 2 keV/nm. An important outcome of our work is the possibility to fabricate optical waveguides in the electronic stopping regime. As for $LiNbO_3$ they may present a number of advantages in comparison to those fabricated by ion implantation.

Acknowledgements

This work has been supported by Madrid Community through the project TECHNOFUSION (S2009/ENE-1679) and by The Spanish Ministry of Science and Innovation under Project MAT-2008-06794-C03-03.

F. Agulló-López, F. Agulló-Rueda, J.M. Cabrera, Electrooptics. Phenomena, Materials and Applications, Academic Press, 1994.
D.L. Griscom, Phys. Rev. B 20 (1979) 1823. 22 (1980) 4192.
F. Agulló-López, R.C. Catlow, P.D. Townsend, Point Defect in Materials, Academic Press, 1984.
R.A. Weeks, R.H. Magruder III, A. Stesmans, J. Non-Cryst. Solids 354 (2008) 208.
S. Klaumünzer, Nucl. Instr. Meth. Phys. Res. B 225 (2004) 136.
P. Kluth, C.S. Schnnohr, O.H. Pakarinen, F. Djurabekova, D.J. Sprouster, R. Giulian, M.C. Ridgway, A.P. Byrne, C. Trautmann, D.J. Cookson, K. Nordlund, M. Toulemonde, Phys. Rev. Lett. 101 (2008) 175503.
A. Meftah, F. Brisard, J.M. Constantini, E. Dooryhee, M. Hage-Ali, M. Hervieu, J.P. Stoquert, F. Studer, M. Toulemonde, Phys. Rev. B 49 (1994) 12457.
J. Manzano, J. Olivares, F. Agulló-López, M.L. Crespillo, A. Moroño, E. Hodgson, Nucl. Instr. Meth. Phys. Res. B 268 (2010) 3147.
F. Chen, X.L. Wang, K.M. Wang, Opt. Mater. 29 (2007) 1523.
M. Toulemonde, S.M.M. Ramos, H. Bernas, C. Clero, B. Canut, J. Chaumont, C. Trautmann, Nucl. Instr. Meth. Phys. Res. B 178 (2001) 331.
A. García-Navarro, F. Agulló-López, M. Bianconi, J. Olivares, G. García, J. Appl. Phys. 101 (2007) 083506.
M. Bianconi, G.G. Bentini, M. Chiarini, P. De Incola, G.B. Montanari, A. Nubile, S. Sugliani, Nucl. Instr. Meth. Phys. Res. B 267 (2009) 2839.
J. Olivares, G. García, A. García–Navarro, F. Agulló-López, O. Caballero, A. García-Cabañes, Appl. Phys. Lett. 86 (2005) 183501.
C.A. Merchant, P. Scrutton, S. Garcia-Blanco, C. Hnatovsky, R.S. Taylor, A. Garcia-Navarro, G. Garcia, F. Agullo-Lopez, J. Olivares, A.S. Helmy, J.S. Aitchison, IEEE J. Quant. Electron. 45 (2009) 373.
L.C. Feldman, J.W. Mayer, S.T. Picraux, Materials Analysis by Ion Channeling, Academic Press, Inc.,, New York, 1982.
K.S. Chiang, J. Lightwave Technol. 3 (2) (1985) 385.
A. Rivera, M.L. Crespillo, J. Olivares, G. García, F. Agulló-López, Nucl. Instr. Meth. B 268 (2010) 2249.
A. Rivera, J. Olivares, G. García, J.M. Cabrera, F. Agulló-Rueda, F. Agulló-López, Phys. Stat. Solidi A 206 (2009) 1109.
F. Agulló-López, A. Méndez, G. García, J. Olivares, J.M. Cabrera, Phys. Rev. B 74 (2006) 174109.
A. Rivera, J. Olivares, M. Crespillo, G. García, M. Bianconi, F. Agulló-López, Nucl. Instr. Meth. B 267 (2009) 1460–1463.
R.M. Van Ginhoven, H. Jonsson, L.R. Corrales, J. Non-Cryst. Solids 352 (2006) 2589.